Research Article Vol. 59, No. 34 / 1 December 2020 / Applied Optics 10729

Reflective Toraldo pupil for high-resolution millimeter-wave astronomy

Alexey Shitvov,[1,*] Giampaolo Pisano,[1,2] Luca Olmi,[3] Pietro Bolli,[3] and Carole Tucker[1]

[1]School of Physics and Astronomy, Cardiff University—Queen's Buildings North, The Parade, Cardiff, CF24 3AA, UK
[2]Dipartimento di Fisica, Sapienza Università di Roma, Piazzale Aldo Moro 2, 00185 Roma, Italy
[3]Osservatorio Astrofisico di Arcetri, Istituto Nazionale di Astrofisica (INAF), Largo E. Fermi 5, 50125 Firenze, Italy
*Corresponding author: ShitvovA@cardiff.ac.uk

Received 7 August 2020; revised 16 October 2020; accepted 16 October 2020; posted 16 October 2020 (Doc. ID 403490); published 30 November 2020

A novel, to the best of our knowledge, beam-shaping reflective surface for high-resolution millimeter/submillimeter-wave astronomy instruments is presented. The reflector design is based on Toraldo's super-resolution principle and implemented with annulated binary-phase coronae structure inspired by the achromatic magnetic mirror approach. A thin, less than half a free-space wavelength, reflective Toraldo pupil device operated in the W-band has been fabricated using mesh-filter technology developed at Cardiff University. The device has been characterized on a quasi-optical test bench and demonstrated expected reduction of the beam width upon reflection at oblique incidence, while featuring a sidelobe level lower than −10 dB. The proposed reflective Toraldo pupil structure can be easily scaled for upper millimeter and infrared frequency bands as well as designed to transform a Gaussian beam into a flat-top beam with extremely low sidelobe level.

https://doi.org/10.1364/AO.403490

1. INTRODUCTION

Historically, the pathway to high-resolution millimeter and submillimeter astronomy has been perceived as continuous increase of the aperture and size of the optical elements. The emerging instruments for high-resolution fast-imaging observations in millimeter- and submillimeter-wave astronomy are equipped with large-diameter cameras that can image large areas of the sky and trace the structures ranging in size from individual comets to the galaxies [1–3]. An alternative to increasing instrument size and cost, and a potentially complementary approach for high-resolution astronomy, is based on the concept of point-spread function (PSF) engineering as a means of transcending the resolution limit of conventional optics [4,5].

Super-resolution induced by optical diffraction with the aid of pupil filters has been a topic of extensive research in visible-light and infrared astronomy for decades [5]. This approach belongs to a class of methods aimed at shaping the PSF while keeping the spatial frequency bandwidth unchanged, [6]. It has been conjectured that diffractive narrowing of the main lobe of the illuminating PSF and, as such, reduction of the inner working angle of the instrument, can lead to improved resolution of point sources. Essentially, diffraction-based super-resolution implies the principle of information capacity invariance, leading to the fundamental trade-offs in terms of Strehl ratio and field of view versus the sidelobe level (SLL). Obviously, implementation of super-resolution for astronomical applications is constrained by the requirement that the new optical elements must have a minimal impact on the receiver's layout and telescope structure.

Recently, spatial filtering with the aid of binary phase pupil masks, particularly those based on Toraldo's super-resolution principle [7], has been explored as a means of achieving resolution beyond the conventional resolution limit in microwave and millimeter-wave optical systems [8–11]. Specifically, it was shown that by patterning the pupil area in a set of concentric annular coronae with piecewise-uniform complex transmittance, a band-limited transverse diffraction pattern of arbitrary shape can be achieved. The main design parameters include the number of coronae and their width, which is sufficient for the transversal PSF shaping [12]. It was also demonstrated that the binary phase masks with constant real transmittance can suit many applications in high-resolution astronomy and microscopy [13]. The axial PSF shaping based on Toraldo pupil synthesis was further developed in [14,15] to enable the complete 3D super-resolution. It appeared that using the phase-only pupil masks can increase the axial resolution by a factor of 2, while providing acceptable Strehl ratio and keeping the

sidelobes at arbitrary low level. The feasibility of wavefront tailoring using polarization-mask apertures was discussed in [16], and it was found that the technique is feasible for focal-shift and partial aberration compensation.

Alongside the development of transmissive pupil filters for refractive optics, diffractive mirrors proved to be a feasible solution for reflective optics, particularly for correcting optical aberrations [17] and generating millimeter-wave vortex beams [18]. In the meantime, the mirror can be made flat using the design approach based on the stacked metal-mesh metasurfaces. In this respect, a number of metamirrors and reflectarrays have been proposed recently, demonstrating anomalous and retroreflection as well as arbitrary beam shaping [19,20]. Despite the remarkable properties, their synthesis is very involved, while their slender performance in terms of the bandwidth and loss deters their immediate application in millimeter/submillimeter astronomy. For instance, the flat focusing mirror proposed in [21] enables photonic imaging of arbitrary light patterns, although it obeys the conventional resolution limit.

In our previous report [22], we briefly discussed the feasibility of using a millimeter-wave metal-mesh metamaterial approach to design transmissive pupil masks for arbitrary amplitude and phase apodization (by *pupil apodization* we shall hereby mean shaping the point-spread function by varying amplitude and/or phase transmission in the entrance pupil of the telescope [5].) Also, a new idea for a simple W-band reflective Toraldo pupil was outlined, inspired by the achromatic magnetic mirror concept, based on the reflection at the interface of materials with high and low dielectric constant (Dk), along with preliminary simulation and measurement results. Previously in [8], a conceptually similar design approach based on the first-order scalar diffraction theory was employed, but the device based thereupon was a transmissive pupil, in contrast to the reflective pupil presented in [11] and in our new paper. In [11], the embedded reflective pupil identical to that in the current work was presented for the first time. However, detailed description of the device theory and analytical-numerical design were omitted. Moreover, experimental characterization in [11] was carried out in a diverging beam, and the resulting beam exhibited low gaussicity, whereas in the current work the device characterization has been conducted with a new quasi-optical feed, placing the beam waist of the incident Gaussian beam at the center of the pupil. As such, this paper significantly extends our previous effort, both in modelling and experimental characterization, and is organized as follows. In Section 2, we introduce the theory of the new reflective Toraldo pupil device, the first-order diffraction modeling approach, and the design based thereupon. The device fabrication and experimental characterization using a quasi-optical test bench are reported in Section 3. The implications for further research and a route for millimeter-wave metamaterial pupil masks are discussed in Section 5.

2. TORALDO PUPIL DESIGN

A. Transmissive Toraldo Pupil Theory

Our design of the reflective Toraldo pupil stems from the classical problem of diffraction of a scalar field on an annular aperture cut in a perfect electric (PEC) conductor screen, and it follows the principle of the transmissive device discussed in [9,10]. Using the Huygens–Fresnel diffraction formula for electrically large aperture in the far-field approximation, e.g., [22], the Fraunhofer diffraction equation for the scalar field $U(x)$ transmitted through an annular circular aperture (corona) illuminated by the field of a uniform plane wave at normal incidence reads

$$U(x) = -\frac{i}{\lambda} \cdot \frac{\pi D^2}{x} \cdot A \cdot [J_1(x) - \rho J_1(\rho x)] \cdot \frac{e^{ikr_0}}{r_0}, \quad (1)$$

where $x = \pi \frac{D}{\lambda} \sin(\phi)$; λ is the free-space wavelength and k is the corresponding wavenumber; D is the outer diameter of the annular aperture and ρD is its inner diameter; ϕ is the angular direction to the observation point (scan angle); A is the amplitude of the incident field on the aperture; $J_1(x)$ is the Bessel function of the first kind of order one; and r_0 is the radial distance to the observation point. The first factor in Eq. (1) constitutes the fact that each equivalent Huygens source within the aperture is represented by a driven dipole, while the last exponential factor indicates the spherical wave emanated by the Huygens sources. If one plots the field amplitude $U(x)$ in Eq. (1) versus the scan angle, they will be able to observe simultaneous beam narrowing (which thereupon we shall consider the principal super-resolution metric) and rising sidelobes as the relative diameter ρ increases. Therefore, one would naturally wonder whether multiple concentric annular apertures (see the five-coronae pupil example in Fig. 1) can help increase the throughput and beam-forming power of the structure, while providing more degrees of freedom for the design.

In fact, the power throughput can be increased by making all annular partitions transparent [13]. Assuming a uniform amplitude distribution over each annular segment and using Eq. (1), the following equation can be readily derived for an M-coronae pupil partitioned by the circles of diameter $\rho_j D (\rho_j \in [0, 1], j = 0, 1, \ldots, M$ and $\rho_0 = 0$ & $\rho_M = 1)$ [23]:

$$U(x) = \sum_{m=1}^{M} -\frac{i}{\lambda} \cdot \frac{\pi D^2}{x} \cdot A_m \cdot [\rho_m J_1(\rho_m x) - \rho_{m-1} J_1(\rho_{m-1} x)] \cdot \frac{e^{ikr_0}}{r_0}. \quad (2)$$

By a judicious choice of the pupil partitioning, optimal super-resolution can be achieved for tolerable sidelobe level. For example, in [10], the analytical synthesis routine based on Eq. (2) required specified coronae diameters and desired positions of zeros in the beam pattern, so that Eq. (2) would yield a system of linear equations for unknown aperture amplitudes A_m. These amplitudes can appear as either positive or negative numbers, defining desired piecewise continuous amplitude and binary phase distribution across the pupil. For a passive structure like the one reported in this work, intentional amplitude apodization would inevitably lead to a lower transmittance. However, the edge taper of the illuminating Gaussian beam may also be incorporated in design.

An example of synthesis of a five-coronae transmissive pupil using Eq. (2) with constraints imposed on the full width at half-maximum (FWHM) and SLL is shown in Table 1 and Fig. 2. Hereafter we assume the design reference frequency for modeling and simulations to be 100 GHz, leaving detailed study of

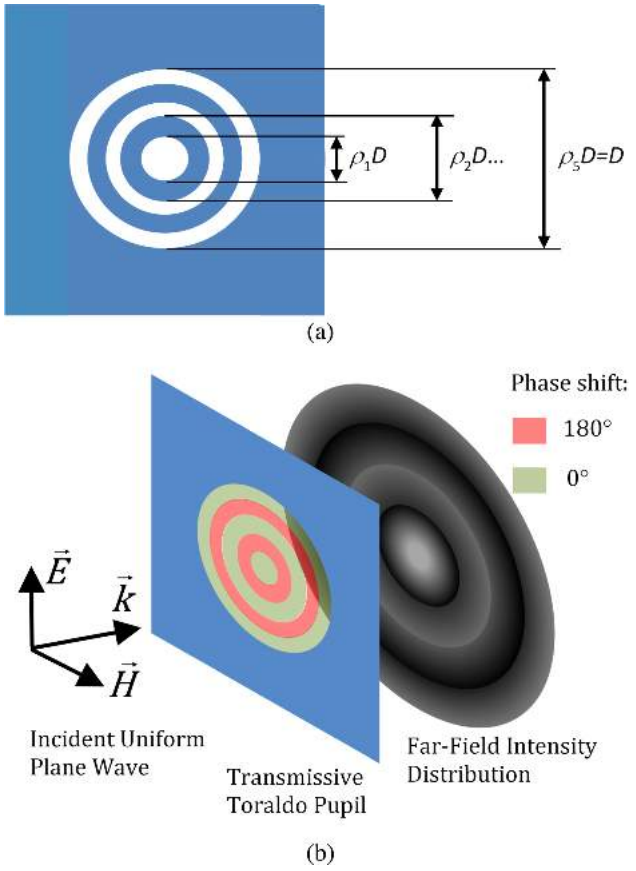

Fig. 1. Transmissive pupil structure: (a) conventional five-coronae transmissive pupil pattern with the shaded blue areas indicating opaque surface interspersed with transparent annular apertures; (b) Toraldo pupil structure with the transparent corona imparting alternate phase shift of 0° (green) and 180° (red) and the opaque area (blue) defining the outer diameter of the pupil.

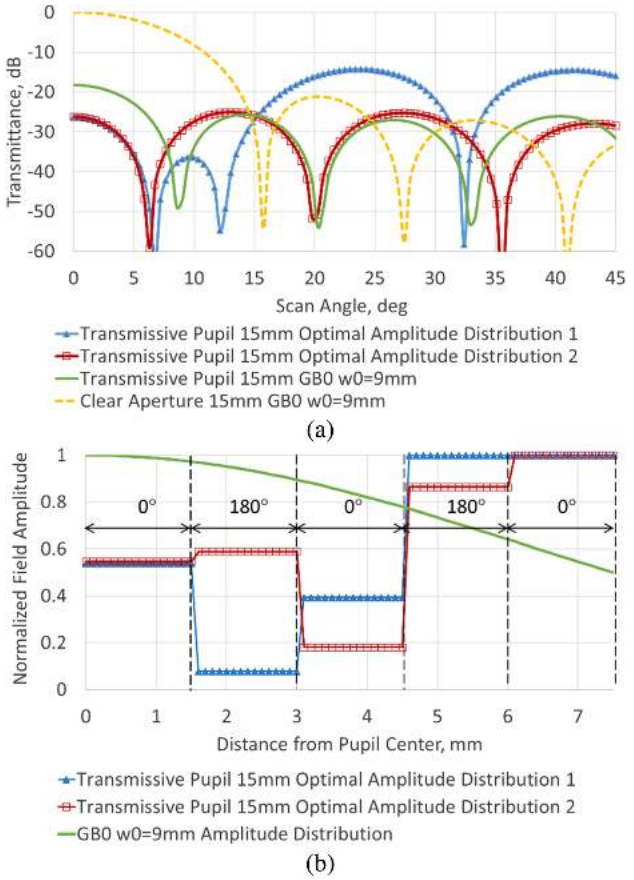

Fig. 2. Numerical example of diffractive super-resolution with a five-coronae transmissive pupil at 100 GHz [Fig. 1(a)], calculated using Eq. (2): (a) normalized (to the clear aperture transmittance at 0°) beam patterns of a 9 mm fundamental-mode Gaussian beam (GB0) transmitted through a clear 15 mm circular aperture (dashed line) and through the five-coronae pupil (solid line without symbols), alongside the beam patterns generated by the piecewise-continuous optimal amplitude distributions (solid lines with symbols) and binary phase distribution across the coronae; (b) optimal amplitude distributions on the coronae against the amplitude distribution corresponding to 9 mm Gaussian beam incident on the pupil.

Table 1. Optimal Five-coronae Transmissive Pupil Designs (Pupil Diameter $D = 15$ mm, Equal Coronae Width)

Design #	Constrained	Un-constrained	Design Parameters
Optimal amplitude distribution 1	50% reduced FWHM; First SLL < -10 dB	High-order sidelobes	Coronae amplitude distribution
Optimal amplitude distribution 2	50% reduced FWHM; Minimum SLL	N/A	Coronae amplitude distribution

the frequency performance of the structure to our future work. The five-coronae pupil has the outer diameter $D = 15$ mm and the relative coronae diameters $\rho_0 = 0$, $\rho_1 = 0.2$, $\rho_2 = 0.4$, $\rho_3 = 0.6$, $\rho_4 = 0.8$, and $\rho_5 = 1$. These dimensions are related to the reflective pupil structure and devised as discussed further in Section 2.B. It is noteworthy that the above set of the relative coronae diameters is suboptimal and can be used as a degree of freedom in optimum design.

In our experiment setup described in Section 3, the pupil is illuminated by a Gaussian beam produced by a quasi-optical feed network, with its beam waist of 9 mm positioned at the center of the pupil, and therefore we use this setup as the reference case. Accordingly, two of the beam patterns in Figs. 2(a) and 2(b) correspond to the Gaussian beam transmitted through the clear 15 mm circular aperture and through the five-coronae pupil aperture, where in the latter case we allow the coronae to be fully transparent apart from the alternating phase inversion imparted on the incident beam. As one can observe from in Figs. 2(a) and 2(b), the alternating binary phase variation causes the main beam narrowing and sidelobe growth, due to both phase change and quantization (due to the piecewise-constant approximation used) errors. Amplitude apodization should allow additional degree of freedom in super-resolution, and two design examples are compared next; see Table 1.

The principal objective of the pupil design is to achieve smaller main beam width while keeping the other characteristics of the beam pattern, such as the boresight gain and SLL, in compliance with the application requirements. Indeed,

super-resolution comes at the expense of the gain and SLL deterioration, as one can clearly see from the modeling of the fundamental-mode Gaussian beam (denoted by "GB0") transmission in Fig. 2(a). The peak intensity at the boresight for the Gaussian beam transmitted through the five-coronae binary-phase pupil decreases by ∼18 dB as compared with the unobstructed aperture. The optimal amplitude apodization further decreases the Strehl ratio by ∼8 dB. This still could be tolerable in some applications. Obviously, pushing the sidelobes beyond the field of view of the instrument thus reducing the signal-to-noise ratio, or, alternatively, reducing the field of view to trim the high sidelobes using an aperture stop—in either case, the trade-off is inevitable and unfavorable for system performance, according to the principle of invariance of information capacity [6,12].

To further reduce the main beam width, one can adjust the field amplitude profile across the aperture, e.g., by introducing piecewise uniform attenuation on the coronae. In the first instance of the transmissive pupil design in Fig. 2, targeting 50% reduction of the FWHM, the nearest side lobe is required to be more than 10 dB below the main lobe, while the higher-order sidelobes are required to be as low as possible. In the second case, no requirement is set for the nearest sidelobe, whereas the overall sidelobe level is minimized by judicious selection of the coronae amplitude profile. The respective amplitude profiles are shown in Fig. 2(b), while the phase alternates by 180° between the adjacent coronae. Obviously, any attempt to reduce the beam width of the main lobe with simultaneous control of the sidelobes results in redirection of radiation into the sidelobes (i.e., reduced intensity of the image spot) and requires complicated amplitude distribution across the pupil (necessary for placing the nulls on the beam pattern), which for a passive structure implies variable attenuation resulting in waste of signal power. On the other hand, the Gaussian beam transmitted through the pupil exhibits ∼34% reduction of the main beam width with the nearest sidelobe level, ∼ −7.3 dB. This is deemed sufficient for demonstration of super-resolution, and we adopted a Gaussian beam illumination profile for the reflective pupil design. It is noteworthy that further reduction of excessively high sidelobes can be achieved by deconvolution in specific applications, e.g., astronomical mapping [24].

B. Reflective Toraldo Pupil Design

In this section, we present in detail the design of a prototype reflective pupil aimed to demonstrate 30% reduction of FWHM and SLL < -10 dB at 100 GHz. The working principle of the reflective pupil discussed in this paper is based upon the achromatic magnetic mirror [25]; see Fig. 3(a). Accordingly, the pupil area is subdivided into a set of concentric coronae with reciprocal phase of the reflection. Reflection from the PEC surface imparts a 180° phase shift on the electric field. The reciprocal, viz. 0°, phase shift is implemented by reflection from the planar interface between a high-impedance, i.e., high dielectric constant, dielectric half-space and a low-impedance dielectric half-space as the wave approaches the interface from the high-impedance medium; see Fig. 3(a). The distance from the dielectric interface to the PEC back-short, approximately

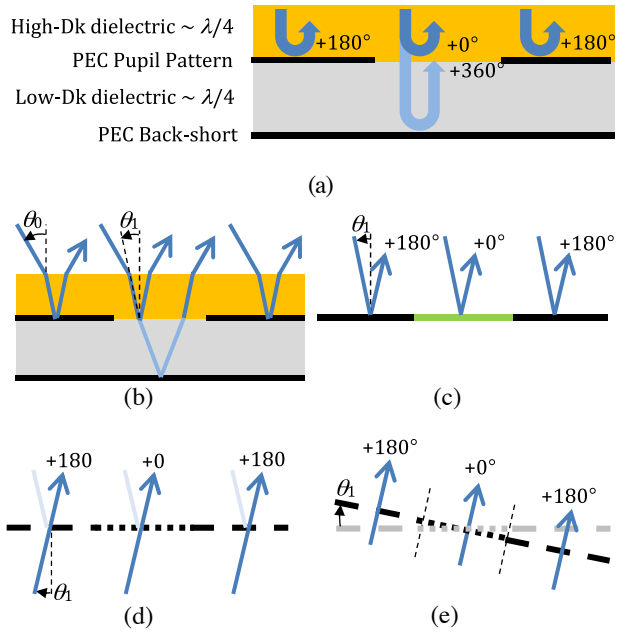

Fig. 3. Principles involved in the design of reflective Toraldo pupil: (a) cross-sectional view of a segment of embedded magnetic mirror with figures in degrees indicating the phase shift imparted upon reflection and transmission through the substrate with a low dielectric constant (Dk); reduction of the ray-tracing model of the reflective pupil to the representative transmissive model showing (b) the physical structure of the reflective pupil, (c) down-sizing of the physical structure to a sheet model, (d) conversion of the reflecting interface into equivalent transmissive one, and (e) mapping of the patterned interface onto the plane orthogonal to the beam axis.

equal to quarter of a wavelength in the low-impedance dielectric substrate, defines the operating frequency of the device. The area outside the pupil diameter should be, in principle, non-reflecting, i.e., either transparent or absorbing, and thus defining the pupil diameter D.

The multi-annular pupil model [Eq. (2)], derived for the transmissive device, can be adopted for the first-order analysis and synthesis of the reflective pupil at oblique incidence. The reflective device geometry can be reduced to a representative transmissive model as shown in Figs. 3(b)–3(e). Therefore, the analytical-numerical design procedure can start by using Eq. (2) to synthesize the planar transmissive pupil geometry, which is then mapped onto specified reflection plane and expanded into a three-dimensional physical structure. The final adjustment of the geometry, aimed to account for the effect of shadowing by the pupil pattern above the ground plane, is carried out using full-wave electromagnetic simulations. If the source field is predetermined, e.g., a Gaussian beam, Eq. (2) can be used for the first-order pupil synthesis with the coronae diameters as the design parameters. The case of the Gaussian beam incident on the reflective pupil is demonstrated in Figs. 4 and 5.

The reflective pupil model [Eq. (2)] employed in Fig. 4 has the central patterned area of 15 mm diameter of the same profile as that of the five-coronae transmissive pupil discussed above, c.f., Fig. 1(a). However, the wide outer area is now set to be reflective. This effectively makes the device a six-coronae reflective pupil. The outer diameter is set to $D = 60$ mm, and

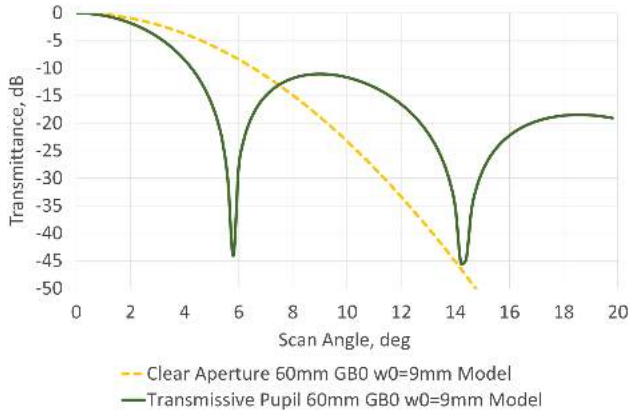

Fig. 4. Analysis of the equivalent transmissive pupil using the analytical model [Eq. (2)] with the inner pattern diameter of 15 mm, outer device diameter of 60 mm, and Gaussian beam waist of 9 mm; see Fig. 5(a). The inner coronae dimensions are the same as those in Fig. 2. The curves are normalized to the respective level at 0°.

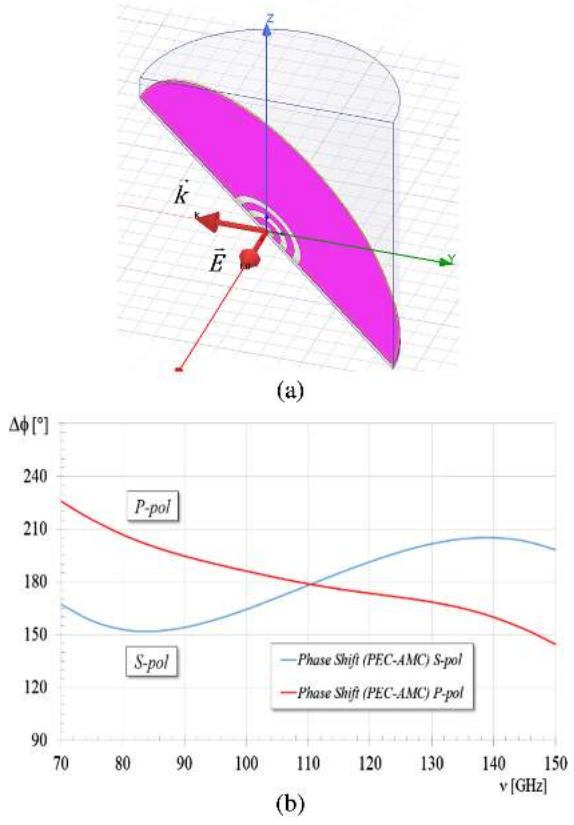

Fig. 5. Design of the super-resolution reflective pupil (outer diameter $D = 60$ mm, inner coronae largest diameter 15 mm) when the aperture illumination is determined by a Gaussian beam incident at 45° with its 9 mm beam- waist positioned at the center of the pupil: (a) the Ansys HFSS model featuring the "Perfect E" symmetry plane (the $Y-Z$ plane) and cylindrical far-field integration surface; (b) the differential phase of reflection from the embedded conductor, i.e., perfect electric conductor (PEC), relative to the internal dielectric interface, i.e., artificial magnetic conductor (AMC), for the *s*- and *p*-polarized Gaussian beams.

the pupil is illuminated by a 9 mm Gaussian beam at 45° skew incidence; see Fig. 5(a). The above choice of the outer diameter provided a deep edge taper of the beam, reasonable model size, and convergence of the results with respect to the finite-element mesh size and further increase of the diameter. Concerning the specific choice of the inner coronae diameters, this was partly empirical but also informed by the modeling. Essentially, we specified the source beam waist to be 9 mm, which was about 2 times the beam waist of the corrugated feed horn available for the experiment and suited the available beam-transformation lens and space on the test bed. The outer diameter of the fifth corona of the reflective pupil was specified at 15 mm, which corresponded to a 6 dB edge taper for the 9 mm beam waist. We note that both the source beam waist and the edge taper figures were circumstantial choice. By requiring all inner coronae to have equal width, the parameter space for Eq. (2) is reduced to a single scaling factor. Running a coarse parameter sweep with finite-element simulation, we found the optimum value of the scaling factor corresponding to a 30% reduction of FWHM and SLL < -10 dB.

The plots in Fig. 4 show a 9 mm Gaussian beam transmitted through the clear 60 mm circular aperture and through the transmissive pupil with the coronae diameters specified as above. Some 30% reduction of the FWHM is observed in the case of the pupil aperture with respect to the clear aperture, with the maximum SLL of -11 dB corresponding to the nearest sidelobe. It is noteworthy that the SLL can, in principle, be further reduced, at the expense of the increasing beam width, by individually varying diameters of the four central coronae with fixed diameter of the fifth corona (15 mm), but this was not deemed to be essential for the demonstration of super-resolution.

A trimetric view of the finite-element analysis (FEA) model implemented with the Ansys HFSS software [26] is shown in Fig. 5(a). The beam waist of the source beam is located at the center of the pupil in the $X-Z$ plane. The linear polarization is set either along the X axis (*s* polarization) or Z axis (*p* polarization). The change of the phase for the beam reflected from the embedded metallic layer and from unobstructed interface between the low-index [porous polytetrafluoroethylene (pPTFE), reference refractive index $n_l = 1.23$] and high-index [polypropylene (PP), $n_h = 1.49$] dielectrics is shown in Fig. 5(b) across the W-band. We note that the model employed for optimization in Fig. 5(b) is that of a uniform interface, i.e., without the pupil pattern, above the infinite ground plane at 45° incidence, where the thicknesses of the high-index and low-index dielectrics were adjusted for the maximum flatness of the phase.

The simulations of the optimized reflective pupil are shown in Fig. 6. The model comprised the elliptical pupil structure [see Fig. 5(a)] represented by the prototype circular pupil with the outer diameter of 60 mm rotated and elongated in one direction to maintain the circular projection onto the plane orthogonal to the incident beam. The sheet PEC model was used for the conductor layers, and radiating boundary conditions were set around the volume encompassing the device and reflected beam. A field source with fundamental-mode Gaussian beam distribution in the $X-Z$ plane [Fig. 5(a)] was placed on the Y axis aligned with the incident beam axis. The source beam waist was set to 9 mm at the center of the pupil.